

IIII Semiconductor crystal growth by GHF IIIII
(Review)

Effects of Gravity and Crystal Orientation on the Growth of InGaSb Ternary Alloy Semiconductors - Experiments at the International Space Station and on Earth-

Yasuhuro HAYAKAWA¹, Velu NIRMAL KUMAR¹, Mukannan ARIVANANDHAN², Govindasamy RAJESH¹,
Tadanobu KOYAMA¹, Yoshimi MOMOSE¹, Kaoruho SAKATA³, Tetsuo OZAWA⁴,
Yasunori OKANO^{5,6,1} and Yuko INATOMI^{6,7,1}

Abstract

The manuscript reviews the microgravity experiments carried out onboard the International Space Station (ISS) to study the effects of gravity and orientation on the dissolution and growth properties of InGaSb ternary alloys. To study the effect of gravity, similar growth experiments were conducted under microgravity and normal gravity conditions. The effect of orientation was studied by the growth of InGaSb from (111)A and (111)B faces of GaSb (Ga and Sb faces) under microgravity onboard the ISS. The experimental results revealed that the growth rate was higher with better quality of crystal under microgravity than normal gravity. A model was proposed to explain the higher dissolution of GaSb (111)B than (111)A direction under microgravity. The higher growth rate of InGaSb from GaSb (111)B was found to be because of its higher dissolution of GaSb(111)B feed.

Keyword(s): InGaSb, crystal growth, gravity, crystal orientation, ISS

Received 3 November 2016, Accepted 14 December 2016, Published 31 January 2017

1. Introduction

InGaSb is a III-V ternary alloy that have tunable properties between its binary compounds InSb and GaSb. The lattice constant and wavelength of $\text{In}_x\text{Ga}_{1-x}\text{Sb}$ can be varied in the range 6.096 ~ 6.479 Å and 1.7 ~ 6.8 μm, respectively. The wavelength of InGaSb is in the infrared (IR) region and it can be used as a substrate for IR detector, thermophotovoltaic (TPV) and thermoelectric applications¹⁻⁴. The growth of InGaSb is affected by various parameters including segregation, constitutional super cooling and convection⁵⁻⁷. These typical physical phenomena can be understood by diffusion controlled heat and mass transfer under microgravity⁸⁻¹⁰.

To understand these phenomena our group has performed various microgravity experiments using different space platforms such as air plane, drop tower, space shuttle and recoverable satellite¹¹⁻¹³. The effects of diffusion and Marangoni convection on the mixing of multi-component melts were investigated in the space shuttle experiment¹¹. In the drop tower experiments, in-situ solidification process was observed using a high speed CCD camera¹². The effects of the gravitational direction on the dissolution and growth processes were investigated by inclining the electric furnace on Earth. The flow pattern and composition profiles were calculated as a function of gravity level. The effects of gravity on the shape of liquid-solid interface and composition profiles were clarified by comparing the experimental results in

1. Research Institute of Electronics, Shizuoka University, 3-5-1, Johoku, Naka-ku, Hamamatsu, Shizuoka 432-8011, Japan
2. Centre for Nanoscience and Technology, Anna University, Chennai 600 025, India
3. Chemical System Engineering, University of Tokyo, 5-1-5 Kashiwanoha, Kashiwa, Chiba 277-8568, Japan
4. Department of Electrical Engineering, Shizuoka Institute of Science and Technology, 2200-2, Toyosawa, Fukuroi, Shizuoka 437-8555, Japan
5. Graduate school of Engineering Science, Osaka University, 1-3 Machiganeyama, Osaka 560-8531, Japan
6. Institute of Space and Astronautical Science, Japan Aerospace Exploration Agency, 3-1-1, Yoshinodai, Chuo-ku, Sagami-hara, Kanagawa 252-5210, Japan
7. School of Physical Sciences, SOKENDAI (The Graduate University for Advanced Studies), 3-1-1, Yoshinodai, Chuo-ku, Sagami-hara, Kanagawa 252-5210, Japan

(E-mail: hayakawa.yasuhiro@shizuoka.ac.jp)

the Chinese recoverable satellite and on Earth. Recently Kinoshita et al., grew SiGe crystal onboard the International space station (ISS)^{14,15}. The wettability test of GaSb, InSb and $\text{In}_x\text{Ga}_{1-x}\text{Sb}$ materials with boron nitride (BN), carbon sheet, Quartz and C-103 alloy at higher temperatures were analyzed to check the affinity of the ampoule configuration as a preliminary study to grow InGaSb at the ISS¹⁶. Various numerical investigations were also carried out to understand the growth kinetics^{17,18}. The experimental and numerical results indicated that the shape of growth interface and composition profiles were strongly influenced by gravity.

Though various microgravity experiments were carried out to investigate the growth process of InGaSb ternary alloys, the time period by these space platforms were limited. Among these space platforms, recoverable satellites can provide comparatively longer duration for about a couple of weeks. Within the limited time duration, a few physical properties such as dissolution and multi component mixing during crystal growth were investigated. A thorough investigation to analyze the heat and mass transfer processes requires a long duration space platform. The ISS provides solution for this problem. To analyze the effect of gravity and orientation dependent dissolution and growth properties of InGaSb ternary alloys, the crystal growth experiments were carried out in the Japanese space experimental module “KIBO”, a part in the ISS. These experiments were made in collaboration with Japan Aerospace Exploration Agency (JAXA) through alloy semiconductor project. The purpose of the ‘Alloy Semiconductor’ crystal growth project was to elucidate the factors affecting the crystal growth of a high-quality bulk ternary alloy semiconductor under μG conditions at the ISS. The ‘Alloy Semiconductor project’ involved 8 experiments, 4 under microgravity and 4 under normal gravity conditions. The experimental results were being analyzed comparatively and it was expected to reveal important results in the field of “microgravity materials science”. The findings of the microgravity experiments would be utilized for the growth of good quality ternary alloy semiconductor crystals under normal gravity on Earth. The high quality InGaSb crystals with tunable properties could be used as a substrate material for the fabrication of high speed electronic devices, IR detectors and TPV systems.

This project was selected as one of the 14 candidate missions of the Kibo Second Phase Utilization in 2008. Our group recently studied the effect of gravity and orientation on the growth properties of InGaSb ternary alloys grown at the ISS^{19,20}.

This manuscript reviews the recent microgravity experimental results that revealed the effects of gravity and orientation on the dissolution and growth properties of InGaSb ternary alloys.

2. Experimental Method

A GaSb(111)A/Te-doped InSb/GaSb(111)A and GaSb(111)B/Te-doped InSb/GaSb(111)B sandwich samples were used for the growth of the InGaSb bulk crystal by vertical gradient freezing (VGF) method. GaSb single crystals along the $\langle 111 \rangle$ orientation were grown by the Czochralski method for the preparation of sandwich samples. **Figure 1** shows schematic diagram of VGF method which was employed for the growth experiment.

Before the growth experiment, the temperature gradient of the furnace was calibrated at the ISS. The InGaSb crystals were grown at the ISS and on Earth using a similar heating profile. The ampoule with (GaSb(seed)/InSb/GaSb(feed)) sandwich sample was kept inside the furnace in which temperature gradient was established (**Fig. 1a**). For the growth of InGaSb, the furnace temperature was gradually increased at a rate of $0.06\text{ }^\circ\text{C}/\text{min}$ up to $700\text{ }^\circ\text{C}$. This temperature was maintained as constant for about 107 h. Based on the reference temperature (measured by the thermocouple) and the temperature gradient, the temperature at the GaSb seed interface was determined and controlled.

During the high temperature growth process, InSb melted at its melting point of $525\text{ }^\circ\text{C}$ and GaSb seed and feed crystals were started to dissolve in InSb melt thereby InGaSb solution was formed (**Fig. 1c**). Because of the temperature gradient, solution at the seed interface gets supersaturated and it provides the driving force for the growth of InGaSb from GaSb seed crystal (**Fig. 1d**). Once crystal was started to grow from seed interface, seed dissolution was stopped and further growth was assisted by dissolution of feed crystal at high temperature. Heat pulses were applied during the holding process at particular interval to induce

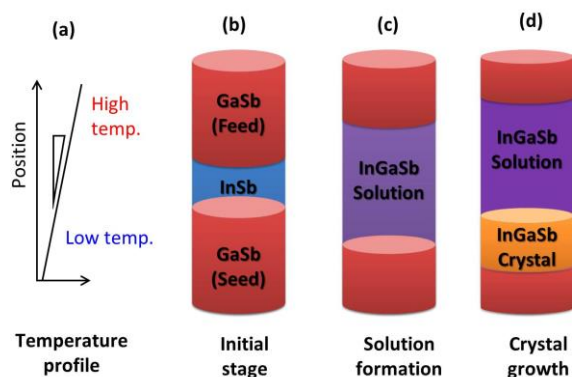


Fig. 1 Schematic diagram of (a) vertical temperature profile, (b) initial stage of sandwich sample, (c) dissolution and (d) growth process of vertical gradient freezing method.

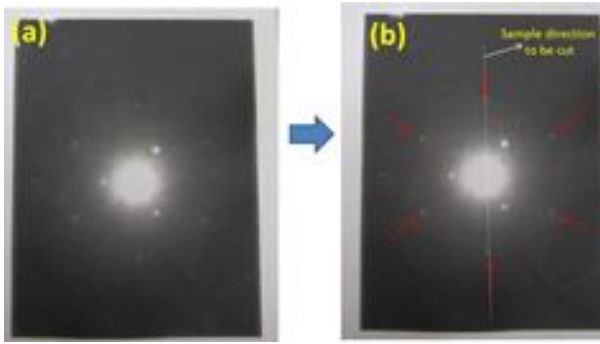


Fig. 2 (a) Laue pattern and (b) cut position of the ampoule with InGaSb crystal.

the growth striations at the growth interface by Te-impurity in melt. The change in temperature modulated the Te-impurity concentration at the growth interface because of segregation of Te impurity. To reveal the modulated Te concentration in the grown InGaSb crystals, an etching process was applied. The etchant HF : CH₃COOH : KMnO₄ in 1:1:1 volume ratio was used to reveal the striations. From the distance between striations, the growth rate was calculated.

A total of 50 heat pulses were applied during the growth period at intervals of 2 h. For clear identification of the striations which are created by heat pulses, the introduction time interval between pulse number 4 and 5 was changed to 1 h. After applying all the pulses, the temperature was decreased to 400 °C at a cooling rate of about 0.5 °C /min to reduce the thermal stress in the grown crystals. Then, the temperature was decreased to room temperature at a cooling rate of about 1 °C /min. A similar experiment was conducted under normal gravity condition to study the effect of gravity on the dissolution and growth process of InGaSb.

The cartridge containing InGaSb sample grown at the ISS was returned to the Earth by a Russian rocket. The grown crystal in the ampoule was taken Laue to fix the cut position along the growth direction (**Fig. 2**). After Laue pattern was recorded, the sample was cut along (110) plane that is perpendicular to growth plane (111) using a diamond saw cutter. One half of the cut sample was used for analyzing its compositional profile and growth properties.

Prior to the analysis, the sample was mirror polished step-by-step using SiC and alumina abrasives of different particle sizes. The mirror polished sample was etched in a 1:3:1 solution of HF: KMnO₄: CH₃COOH for 30 min at room temperature to observe the Te impurity striations and etch pits. The composition profiles, interface shapes, and striations of the grown crystals were analysed by Electron Probe Micro Analysis (EPMA), polarized optical microscopy, and Field Emission Scanning Electron Microscope (FE-SEM).

3. Results and Discussion

3.1 Effect of Gravity

3.1.1 Dissolution of GaSb Seed and Feed Crystals

Figure 3a and **b** show the cross section of μ G and 1 G samples, respectively. The dissolution lengths of crystals were measured from undissolved seed and feed crystals that are given in **Table 1**.

The dissolution lengths of GaSb seed and feed crystals under μ G were 2.3 and 15 mm, respectively, whereas they were 4.9 and 11 mm in the 1 G sample. The dissolution length of the seed crystal was larger in the 1 G sample, whereas the dissolution length of the feed crystal was larger in the μ G sample. The strong convection in the solution causes a large amount of seed dissolution under 1 G, whereas under μ G, the solute transport was diffusion dominant, decreasing the seed dissolution rate, as confirmed by our numerical simulation results²¹). The length of the crystal grown under μ G (14.9 mm) was larger than that of the 1 G sample (12.6 mm) because a larger amount of feed was supplied for growth under diffusive transport compared with the 1 G experiment.

Table 1 Dissolution lengths of GaSb seed and feed crystals under μ G and 1 G conditions.

Sample	Undissolved (dissolved) length in μ G (mm)	Undissolved (dissolved) length in 1G (mm)
Seed	20.7 (2.3)	18.1 (4.9)
Feed	8 (15)	12 (11)

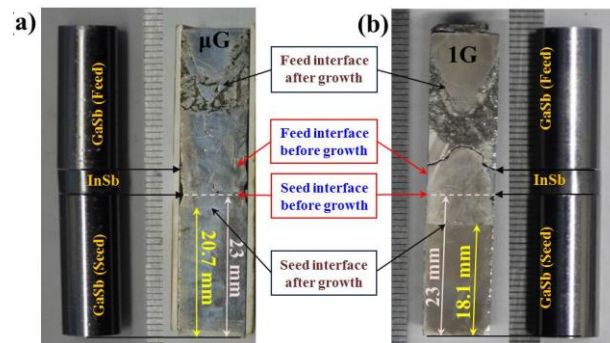


Fig. 3 Sandwich samples before and after experiments (a) under μ G and (b) 1 G. The interface positions of μ G (a) and 1 G samples (b) before and after experiments are indicated.

3.1.2 Growth Rate under μ G and 1 G Conditions

The growth rate was calculated from the striations that were revealed by the etching process. The etched surface of InGaSb crystals near seed interface grown under μ G and 1 G is shown in **Fig. 4a, b** respectively. For clarity, the striations are marked as solid lines in the optical microscopic images of the etched samples. The striations formed by their corresponding heat pulses were marked as p1, p2...etc. Initially, the growth started at the peripheries in the 1G samples, as striations 1 and 2 were observed at the peripheries as shown in **Fig. 4c** and disappeared at the centre. The striations were highly concave, while the initial seed interface was nearly flat with steps at the peripheries. The angle of steps one and two (**Fig. 4d**) are around 70° , which confirmed that both steps were in the (111) plane. This shows that the kinetics played a more dominant role in the dissolution process under 1 G. On the other

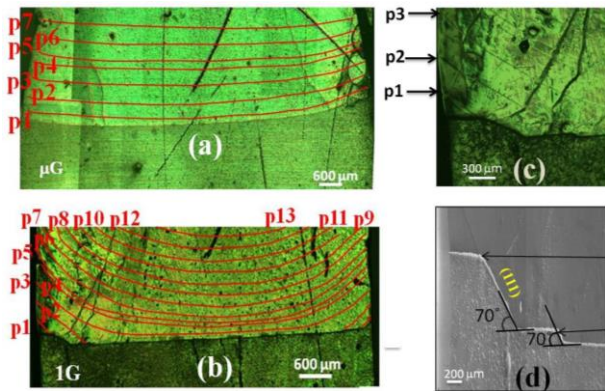


Fig. 4 Polarized optical microscope images of the etched surfaces of (a) μ G and (b) 1 G samples. (c) Optical micrograph and (d) FE-SEM image of the periphery of the 1G sample.

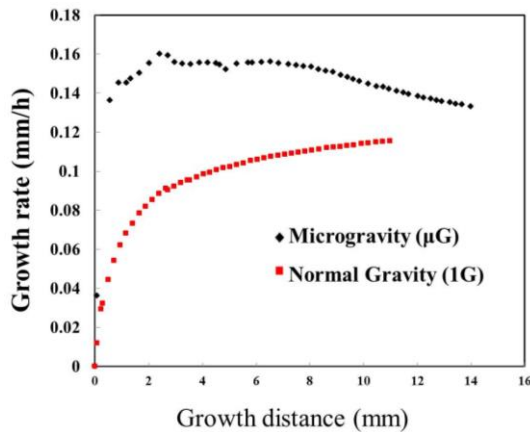


Fig. 5 Growth rate variations of μ G and 1 G samples.

hand, the initial striations were clearly observed at the centre and periphery of the μ G sample, and the shape of the striations resembled the interface shape, which indicated a flat interface (**Fig. 4a**).

By measuring the grown length between the striations, the growth rates of the crystals were measured. **Figure 5** shows the growth rate variation along the growth direction of μ G and 1 G samples. The growth rate of the crystal under μ G was higher than that under 1 G. The growth rate of the μ G sample was 0.135 mm/h at 0.5 mm of grown length, increasing to a maximum of 0.16 mm/h when the grown length reached 2.4 mm, and the growth rate became stable after the grown length of 3 mm. The diffusion-controlled steady state growth continued for the next 6 mm of grown length. Under 1 G, the initial growth rate was one order of magnitude lower than that under μ G, as a rate of 0.04 mm/h was measured at 0.5 mm of grown length of the 1 G sample. The maximum growth rate of 0.11 mm/h was observed at 7.8 mm of grown length, and the diffusion-controlled steady state growth period was only a few mm at the final stage of growth because of the strong convection under 1 G.

The schematic of melt convection and solid diffusion processes under normal and microgravity conditions are shown in **Fig. 6**. The strong convection and vortex at the center causes the solute transport from the center to the periphery under 1 G.

The velocity of the vortex flow is relatively low at the peripheries; thus, the dissolution is smaller at the peripheries. Moreover, the solutes accumulate at the peripheries while the solution at the center remains under saturated because of strong convection. Therefore, the solution at the peripheries becomes supersaturated and the growth is initiated at the peripheries under 1 G. Under μ G, the solute transport is diffusion dominant; the solute is evenly transported from feed to seed, the solution attains

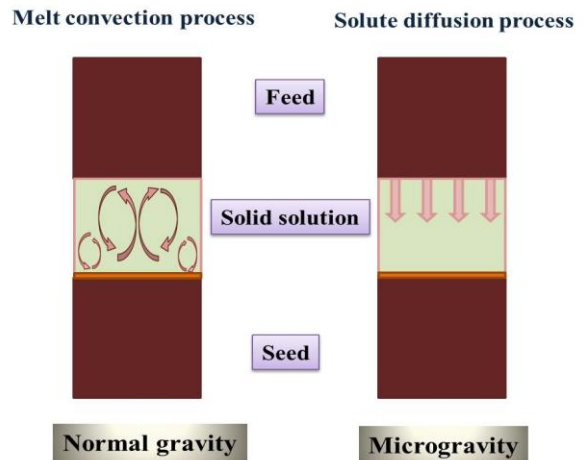


Fig. 6 Schematic of melt convection and solid diffusion processes.

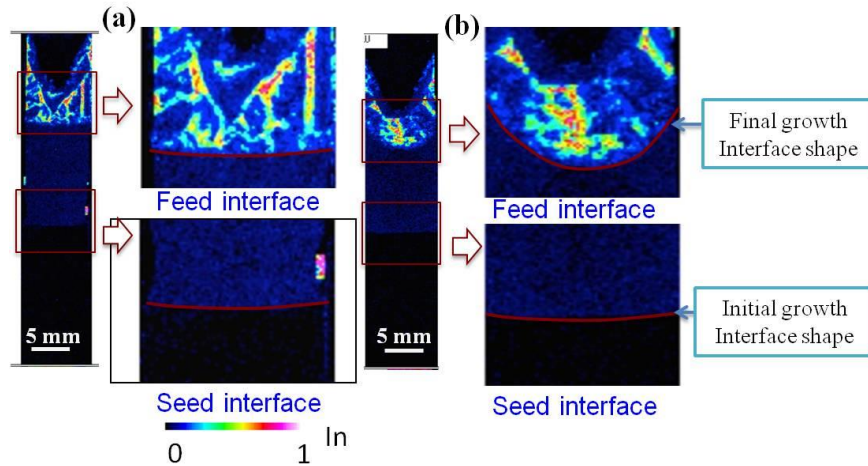


Fig. 7 EPMA mapping of indium distribution in the (a) μG and (b) 1 G samples.

equilibrium at the seed interface, and growth is initiated at the peripheries and centre at nearly the same time. The growth was initiated faster under μG compared to 1 G, as all the striations were observed in the crystals (Fig. 4a), possibly because of the absence of solutal convection. In the 1 G sample, the growth was delayed because of the presence of convection, which hinders the solution from attaining equilibrium. As a result, the initial striations were not observed at the centre of the sample (Fig. 4b).

The solution exhibits two kinds of flows resulting from compositional and temperature variations in the solution. One is the dominant convective flow in the middle region from seed to feed interface that returns to seed interface through periphery. Another weak flow is at the periphery region from seed to feed interface that returns to seed interface through middle. As time elapses, the flow at the periphery region is suppressed by the flow from central region. Therefore, higher amounts of solutes are accumulated at the peripheries. As a consequence, the solution at the periphery becomes supersaturated, leading to the initiation of growth under 1 G condition.

Under microgravity the solutes dissolved at the seed interface were not able to move up to the feed interface unlike the 1 G condition due to the absence of convection and thus the solution at the seed interface gets locally supersaturated. Therefore under microgravity, the growth started earlier than 1 G condition. Moreover, the dissolved solutes from feed interface sturdily diffuse towards seed interfaces due to density gradient between solute and solvent. Therefore, the growth rate is relatively high under microgravity compared to 1 G. Whereas under 1 G, convection is dominant that reduced the solute accumulation near seed interface. Moreover seed dissolution is stopped once crystal was started to grow from seed interface. Hence the initiation of growth was delayed and growth rate was low compared to μG .

3.1.3 Indium Compositional Distribution

Figure 7a and b show the EPMA mapping of indium distribution in the μG and 1 G samples, respectively. The magnified images of indium mapping at seed and feed interfaces of both samples illustrate the variations of the interface shape at the initial and final stages of growth under μG and 1 G. From the mapping, it is clear that the shape of the growth interface of the μG sample remained almost the same from the initial to the final stage of growth. However, the growth interface of the 1 G sample was nearly flat at the initial stage and highly concave toward the feed at the final stage of growth. Moreover, a 'V'-shaped feed interface was observed in both samples beyond the residual solution region.

The indium composition profile of the crystals measured along the growth direction is shown in Fig. 8. The composition profile clearly indicates that $\text{In}_x\text{Ga}_{1-x}\text{Sb}$ crystal grew under μG from 20.2

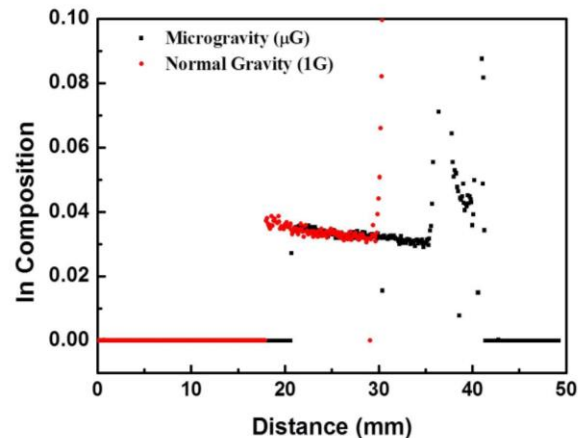


Fig. 8 Indium composition profile of μG and 1 G samples.

to 35.1 mm; thus, the length of the grown crystal was 14.9 mm. However, the crystal grew under 1 G from 18.0 to 30.6 mm, with a grown length of 12.6 mm.

The amount of indium gradually decreased along the growth direction and fluctuated after 35.1 and 30.6 mm in μ G and 1 G samples, respectively. Because the crystal cooled after the growth period, the residual solution rapidly solidified, which caused the compositional fluctuation at the end of growth. As growth proceeds, the growth interface moves towards the high temperature region, leading to a gradual increase in growth temperature in accordance with the temperature gradient. As a result, the relative amount of indium decreased along the grown length.

The indium composition of the μ G sample at the seed interface was 0.028 and gradually decreased along the growth direction. The indium composition of the 1 G sample at the seed interface was 0.041 because of the large amount of seed dissolution, which shifted the interface position towards the low temperature seed end. The indium composition data were converted to growth temperature using an InSb-GaSb binary phase diagram, and the temperature gradient was calculated. The calculated temperature gradient of the μ G sample (0.64 °C/mm) was slightly higher than that of the 1 G sample (0.58 °C/mm), and the calculated values were almost the same during the growth.

3.1.4 Variations in Etch Pit Density

To ascertain the quality of the grown crystals, the etch pit variations in crystals grown under μ G and 1 G were comparatively analysed. **Figure 9a** and **b** show optical micrographs of the etched surfaces of μ G and 1 G samples, respectively. The etch pit density (EPD) was calculated by counting the pits in both samples with respect to seed and grown crystals. The EPD was higher for the seed crystals in both samples because the seed crystals are grown by the Czochralski method at high temperature. The EPD was lower in the grown crystal under μ G ($2.16 \times 10^4/\text{cm}^2$) compared with that grown under 1 G ($2.72 \times 10^4/\text{cm}^2$).

3.2 Effect of Crystal Orientation under Microgravity

InGaSb ternary alloys were grown along the (111)A and (111)B faces of GaSb by the VGF method using sandwich-structured ampoules of GaSb(111)A/InSb/GaSb(111)A and GaSb(111)B/InSb/GaSb(111)B under microgravity condition to study the effects of orientation. Before analysing the samples, the temperature profile of these two experiments were compared.

3.2.1 Temperature Profile

Figure 10 shows the comparison between temperature gradients of (111)A and (111)B experiments. The seed interface temperatures of (111)A and (111)B experiments, at the earlier stage of growth, were found to be 687.3 and 688.2 °C, respectively,

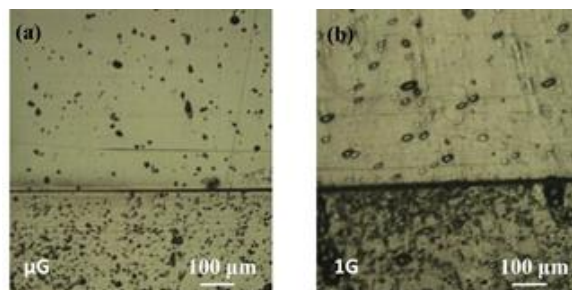


Fig. 9 Optical microscope images of the etched surfaces of (a) μ G and (b) 1 G samples.

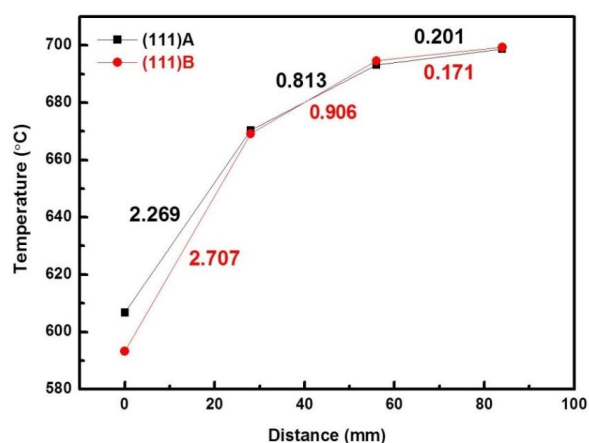


Fig. 10 Comparison between temperature gradients of (111)A (black script) and (111)B (red script) experiments, along the length of the cartridge.

and the temperature gradients were calculated to be 0.81 and 0.90 °C/mm, respectively, from the recorded temperature profile. The (111)B experiment had 11.1 % higher temperature gradient than (111)A.

3.2.2 Dissolution Lengths of Seed and Feed Crystals

The InGaSb samples were cut along the (110) plane, and their EPMA mapping for indium distribution with their initial and final seed and feed interfaces are shown in **Fig. 11(a)** and **(b)**. (Hereafter, InGaSb grown along the (111)A and (111)B faces are denoted (111)A and (111)B samples, respectively). The dissolution lengths of the seed and feed crystals of both (111)A and (111)B samples were calculated from the remaining undissolved crystals.

A total of 2.3 and 2.5 mm of seed crystals, and 14.4 and 19.9 mm of feed crystals, were dissolved in (111)A and (111)B samples, respectively. The initial growth (seed) interface for both (111)A and (111)B samples was almost flat, whereas the feed crystals remained in a “V” shape. Hence, the dissolution length of the feed

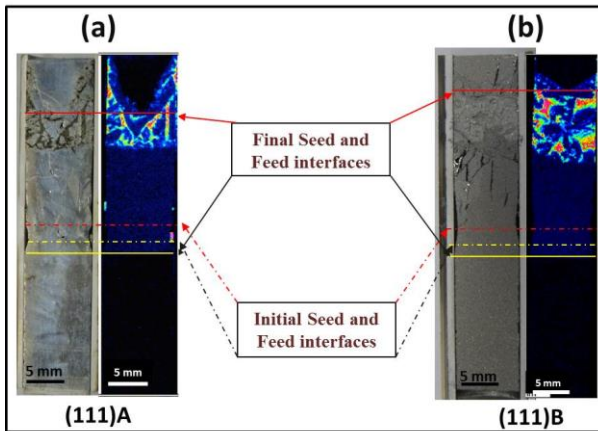


Fig. 11 Cross section and indium composition mapping of InGaSb crystals grown along GaSb (a) (111)A and (b) (111)B faces.

crystal was considered in the middle position rather than the periphery, where more GaSb was dissolved. The remaining indium-rich solution was solidified during the cooling process near the feed crystal in both samples.

From the dissolution lengths of the seed and feed crystals, the dissolution of (111)B was found to be greater than that of (111)A because of the different arrangement of atomic layers. The higher dissolution of the Sb face can be explained based on the atomic arrangement and their binding with the next layer of that plane. The atomic arrangement of GaSb $1 \times 1 \times 1$ cell and $2 \times 2 \times 2$ cells along the (111)A and (111)B faces are shown in **Fig. 12** and **13**. The (111)A face has the arrangement Ga-Sb-Ga-Sb, and the (111)B face has Sb-Ga-Sb-Ga repeated atomic layers. From the figure, it is clear that in a GaSb $1 \times 1 \times 1$ cell, the (111)A face has 6 Ga atoms, 3 at corner and 3 at face-centred positions. The corner Ga atoms were bonded with the next Sb layer with a single bond, whereas the face-centred Ga atoms had 2 bonds with the Sb atoms. In total, 6 Ga atoms were bonded with the next layer, which has 3 Sb atoms, by 9 bonds.

For the (111)B face, a single Sb atom was bonded with the next layer, which has 6 Ga atoms in which 3 face-centred Ga atoms bond with that Sb atom. Considering GaSb $2 \times 2 \times 2$ cells, 10 Ga atoms were bonded with the next atomic layer, which has 6 Sb atoms, in the (111)A face, whereas in the (111)B face, 3 Sb atoms were bonded with 7 of 10 Ga atoms in the next atomic layer.

The number of atoms in each atomic layer and their bonds with the next layer were calculated for $1 \times 1 \times 1$ and $2 \times 2 \times 2$ cells. The calculated number of atoms and bonds in GaSb (111)A and (111)B faces are given in **Table 2**.

The total number of Ga and Sb atoms in the (111)A and (111)B faces were the same for $1 \times 1 \times 1$ and $2 \times 2 \times 2$ cells, whereas the

Table 2 Number of atoms and bonds in the (111)A and (111)B faces of GaSb.

GaSb – $1 \times 1 \times 1$ cell						
Atomic layer	(111)A			(111)B		
	No. of atoms		No. of bonds with next atomic layer	No. of atoms		No. of bonds with next atomic layer
	Ga	Sb		Sb	Ga	
1 st	6		9	1		3
2 nd		3	3	6		3
3 rd	6		3	3		9
4 th		1	1	6		0
Total	12	4	16	4	12	15
GaSb – $2 \times 2 \times 2$ cells						
1 st	10		18	3		9
2 nd		6	6	10		10
3 rd	18		36	10		30
4 th		12	12	18		12
5 th	18		30	12		36
6 th		10	10	18		6
7 th	10		9	6		18
8 th		3	3	10		1
Total	56	31	124	31	56	122

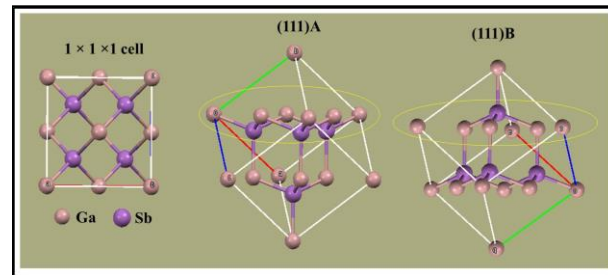


Fig. 12 Atomic arrangement - $1 \times 1 \times 1$ cell of GaSb (111)A and (111)B.

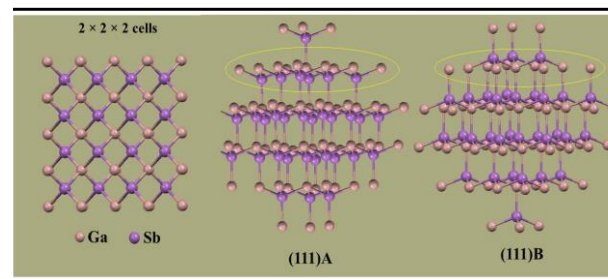


Fig. 13 Atomic arrangement - $2 \times 2 \times 2$ cells of GaSb (111)A and (111)B.

binding between the atoms shows a significant difference. For the $1 \times 1 \times 1$ cell, the (111)A face had 16 bonds, whereas the (111)B face had 15 bonds. In the case of $2 \times 2 \times 2$ cells, the (111)A and (111)B faces had a total number of 124 and 122 bonds, respectively. This shows that the $1 \times 1 \times 1$ cell had 1 excess bond and the $2 \times 2 \times 2$ cells

had 2 excess bonds in their (111)A face. As the number of unit cells increased, the excess bonds in the (111)A face increased.

When we consider a bulk material of $n \times n \times n$ cells, it would have n number of excess bonds in (111)A compared with the (111)B face. In the above mentioned model if we consider that Sb atoms are located at the corner, (111)B face will have more number of atomic bonds than that of (111)A face. However, irrespective of the position of corner atoms, the once face of GaSb(111) had more number of bonds than that of other face. Hence one face of GaSb (111) will dissolve more than that of the other face because less activation energy is required to break the bonds on that face compared with the other face. The experimental results have shown that the (111)B face was dissolved more than that of (111)A face. The consideration of Ga atoms at the corner position in the above mentioned model supports the experimental data and hence, the higher dissolution of GaSb (111)B was because of the less number of atomic bonds on that face. The obtained result was consistent with our previous microgravity experiment.

3.2.3 Indium Composition

The vertical distribution of indium composition was measured at three positions (Periphery – I, Middle and Periphery – II) along the growth direction, and the radial distribution was measured at two positions near the seed and in the middle position. **Figure 14(a)**

and **(c)** show the indium composition along the vertical direction with the measured position of both (111)A and (111)B samples (**Fig. 14d**). The initial indium composition for both the samples was approximately 0.034 and gradually decreased to 0.030 in the (111)A sample, whereas it ended up at 0.026 in the (111)B sample. During the growth process, the growth interface moved towards the high-temperature feed region because the temperature gradient was maintained in the furnace. Hence, the indium composition along the growth region decreased according to the phase diagram. The random distribution of indium in the later stages of growth occurred because of the solidification of residual melt when cooling was applied to the system.

The radial indium composition is shown in **Fig. 15**. The radial distribution of indium was uniform in both samples.

3.2.4 Growth Rate

The etched surfaces of the (111)A and (111)B samples near the growth interface are shown in **Fig. 16**, in which the striations are marked with red lines for clear visibility. The initial growth interface shape was almost flat in both samples, and the striations had a flat interface. The growth rates of the (111)A and (111)B samples were calculated along three vertical positions (Periphery – I, Middle and Periphery – II) by measuring the distances between the induced growth striations.

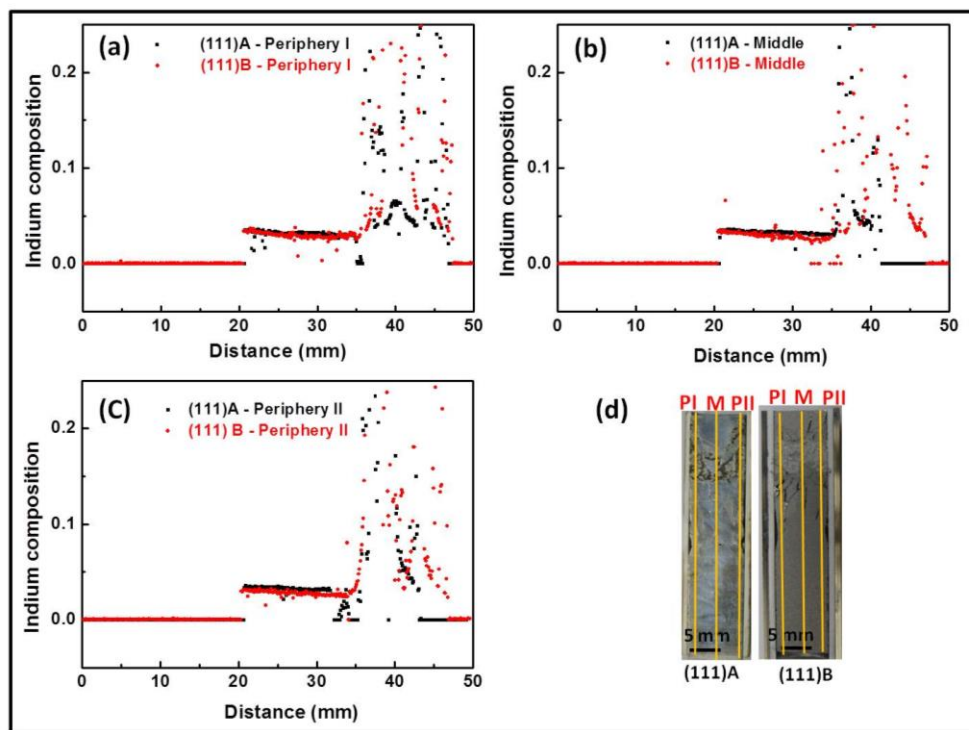


Fig. 14 Indium composition measured by EPMA along the vertical directions (a) periphery – I, (b) middle, (c) periphery – II; and (d) the crystal surface showing the composition measured positions.

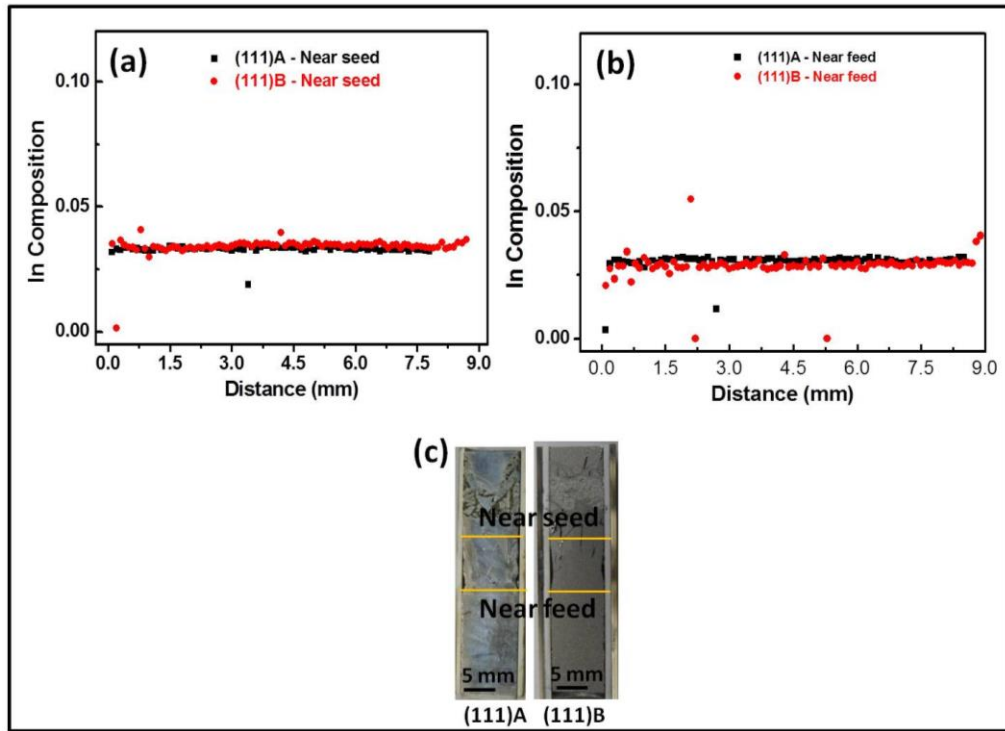


Fig. 15 Indium composition measured by EPMA along the radial directions near the (a) seed interface, (b) feed interface and (c) the crystal surface showing the composition measured positions.

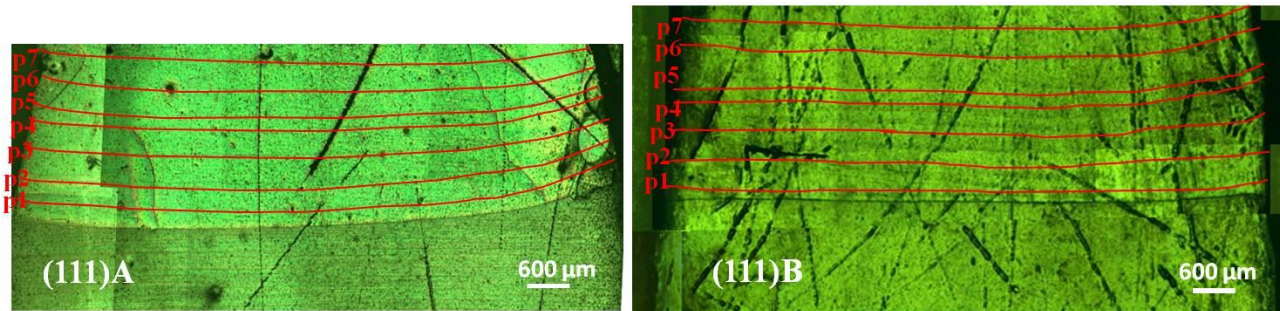


Fig. 16 Initial seed interface shape and striations of (a) (111)A and (b) (111)B samples.

Figure 17 shows the growth rate profiles along three positions: periphery – I (**Fig. 17a**), middle (**Fig. 17b**) and periphery – II (**Fig. 17c**) of (111)A and (111)B samples along with the calculated positions (**Fig. 17d**) of the crystals. The insets of the figures show the initial stage of growth at the corresponding positions. The growth rates at the saturated end (later stage of growth) of (111)A and (111)B samples were 0.13 and 0.15 mm/h, respectively.

The growth rates at various positions along the growth direction indicate that the (111)B face had a higher growth rate than the (111)A face. Even though the growth rate was observed to be

higher for the (111)B sample, the difference between the growth rates was minimum at the initial stage, which would be within the error limit. Hence, at the initial stage, we might not conclude that the growth rate for (111)B was high. However, a higher growth rate was clearly observed in the later stages of the experiment. Moreover, the differences between the growth rates increased from the initial to the final stage, which can be clearly seen in **Figure 17**. It was found that the growth rate of the (111)B face was 15.4 % higher than that of (111)A.

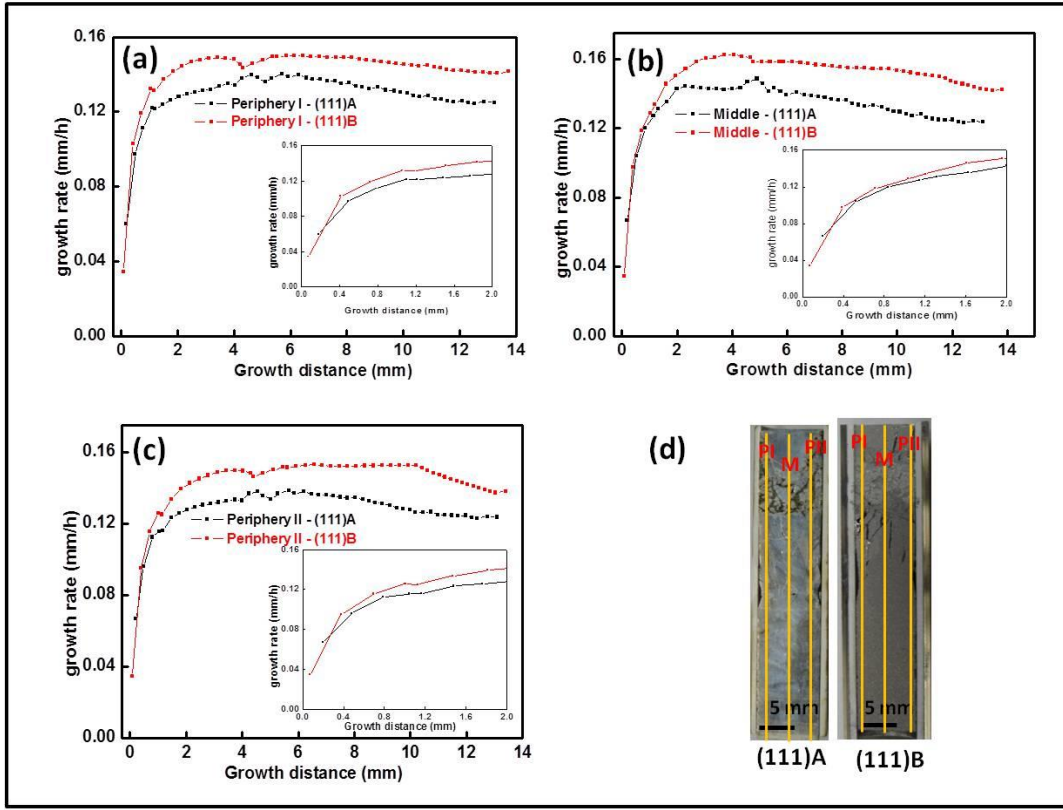


Fig. 17 Growth rates of InGaSb along (a) periphery – I, (b) middle position, (c) periphery – II and (d) Crystal surface showing the growth rates measured positions.

3.2.5 Effect of Temperature Gradient on Growth Rate

Considering that the growth under microgravity by VGF is a diffusion-controlled steady state process and assuming the solute was saturated in the solution, the relationship between the growth rate and solute concentration is given by,

$$V = -\frac{D}{(C_{l0} - C_{s0})} \left(\frac{\partial C_L}{\partial Z} \right)_{Z=0} = -\frac{D}{(C_{l0} - C_{s0})} \left(\frac{\partial C_L}{\partial T} \right) \left(\frac{\partial T}{\partial Z} \right)_{Z=0}, \quad (1)$$

where D = Inter diffusion coefficient between solute and solvent (diffusion coefficient of GaSb under microgravity); $\frac{\partial C_L}{\partial Z}$ = Composition gradient in solution along the distance z ; $\frac{\partial C_L}{\partial T}$ = Reciprocal of the slope of the liquidus line in the InSb-GaSb binary phase diagram; $\frac{\partial T}{\partial Z}$ = Temperature gradient in the solution (i.e., temperature gradient applied to the furnace); and

C_{l0}, C_{s0} = GaSb concentration in solution and that in the crystal at the growth interface, respectively.

In equation (1), the terms D , C_{l0} , and C_{s0} are constants. In the present experiment, the temperature gradient $\left(\frac{\partial T}{\partial Z} \right)$ was attempted to be fixed as a constant, but in the actual case, the (111)B experiment had a temperature gradient $0.09 \text{ }^\circ\text{C/mm}$ higher than that of (111)A. Hence, it was necessary to analyze the effect of the temperature gradient on the growth rates of (111)A and (111)B samples. To accomplish this, the concentration gradient term $\frac{\partial C_L}{\partial T}$ was assumed to be constant for both (111)A and (111)B experiments.

Then, equation (1) can be rewritten as,

$$V = A \left(\frac{\partial T}{\partial Z} \right)_{Z=0}, \quad (2)$$

where $A = -\frac{D}{(C_{l0} - C_{s0})} \left(\frac{\partial C_L}{\partial T} \right)$ is a constant.

Based on equation (2), the growth rate was directly proportional to the temperature gradient.

Let V_1 and V_2 be the growth rates and $\partial T_1/\partial Z$ and $\partial T_2/\partial Z$ be the temperature gradients of the (111)A and (111)B experiments, respectively. Then, the growth rates of the (111)A and (111)B experiments are,

$$V_1 = A \left(\frac{\partial T_1}{\partial Z} \right), \quad (3)$$

$$V_2 = A \left(\frac{\partial T_2}{\partial Z} \right), \quad (4)$$

$$\frac{V_1}{V_2} = \frac{\partial T_1/\partial Z}{\partial T_2/\partial Z}. \quad (5)$$

The above equation shows that the ratio between growth rates should be equal to the ratio between the temperature gradients of the (111)A and (111)B experiments. The experimental results showed that (111)B had a 15.4% higher growth rate and 11.1% higher temperature gradient than (111)A. The ratio of growth rate was higher than that of the temperature gradient. Hence, it is clear that the higher growth rate of the (111)B experiment was not only influenced by the temperature gradient $\left(\frac{\partial T}{\partial Z}\right)$, but also by another factor $\left(\frac{\partial C_L}{\partial T}\right)$. The factor $\frac{\partial C_L}{\partial T}$ depends on the dissolution of the GaSb feed. The dissolution of the GaSb seed was found to be higher in (111)B than (111)A. Hence, the greater amount of solute in the solution resulted in the higher growth rate of (111)B compared with (111)A because of the higher concentration gradient $\left(\frac{\partial C_L}{\partial T}\right)$.

4. Conclusion

$\text{In}_x\text{Ga}_{1-x}\text{Sb}$ alloy crystal was grown under μG onboard ISS using GaSb (111)A/Te-doped InSb/GaSb (111)A and GaSb (111)B/Te-doped InSb/GaSb (111)B sandwich sample by a vertical gradient freezing method. A similar experiment was conducted under 1 G on Earth. The dissolution and growth processes of μG and 1 G samples were comparatively analysed.

(1) Effect of gravity: The kinetics played a dominant role in dissolution process under 1 G, as steps were observed at the peripheries of the seed interface. The seed interface of the μG sample was highly symmetric and slightly concave. The growth started at the peripheries under 1 G, which can be explained using the calculated flow velocity of the solution at high temperature. The growth rate was higher under μG compared with 1 G. The quality of the μG sample was better, as low EPD was observed compared with the 1 G sample. The suppressed convection under μG affected the dissolution and growth process of this alloy semiconductor.

(2) Effect of orientation (under microgravity): The temperature

profiles used for both experiments were similar, and the temperature gradient varied slightly; that is, it was 0.09 °C/mm higher in the (111)B experiment than in the (111)A experiment. The experimental results indicate that the GaSb seed and feed crystals dissolved more along (111)B than (111)A because of the difference in the atomic arrangement of Ga and Sb atoms and their binding with the next atomic layer in their respective planes. The indium composition along the growth direction gradually decreased according to the phase diagram. The difference between the growth rates at the initial stage was very small when compared with the later stages of growth. In a diffusion-controlled growth process under microgravity, the dissolution of GaSb (111)B was higher than that of (111)A and the growth rate of InGaSb ternary alloy from GaSb (111)B was greater than that of GaSb (111)A.

Acknowledgments

This work was financially supported by (1) a Grant-in-Aid for Scientific Research (B) (no.22360316, 25289270, 25289087) and a Grant-in-Aid for Young scientist C (no.22760005) from the Ministry of Education, Culture, Sports, Science and Technology (MEXT) of Japan, (2) JSPS and DST under the Japan–India Science Cooperative Program (Joint Research Project), and (3) the cooperative research projects of the Research Institute of Electronics, Shizuoka University. The authors thank Prof. T. Ishikawa, Prof. S. Yoda, and Mr. M. Takayanagi of the Institute of Space and Astronautical Science, Japan Aerospace Exploration Agency (JAXA) for their support of the related research and fruitful discussion. The authors also thank the GHF experimental operation team and the staff of the Space Environment Utilization Center, HSMD, JAXA for their technical help in microgravity experiments. We thank Prof. M. Kumagawa, Shizuoka University and Prof. T. Nishinaga, University of Tokyo for continuous discussion and suggestion. The Centre for Instrumental Analysis, Shizuoka University, Hamamatsu, Japan provided the characterization facilities.

References

- 1) S. Wang, *Lattice Engineering: Technology and Applications*, Pan Stanford Publishing, Singapore, 2013.
- 2) N.T. Yeh, P.C. Chiu, J.I. Chyi, F. Ren and S. J. Pearton: *J. Mater. Chem., C*, **1** (2013) 4616.
- 3) P.S. Dutta, H.L. Bhat and V. Kumar: *J. Appl. Phys.*, **81** (1997) 5821.
- 4) R. Rogalski and P. Martyniuk: *Infrared Physics & Technology*, **48** (2006) 39.
- 5) P.S. Dutta: *J. Cryst. Growth*, **275** (2005) 106.
- 6) J. Kang and T. Fukuda: *Mater. Sci. Eng., B*, **75** (2000) 149.
- 7) G.M. Blom, T.S. Plaskett, *J. Electrochem. Soc.: Solid State Science*, **118** (1971) 1831.
- 8) G.A. Muller: *J. Cryst. Growth*, **99** (1990) 1242.
- 9) I. Egry: *Materials Transactions*, **45** (2004) 3235.
- 10) L.L. Regel: *Acta Astronautica*, **17** (1988) 1241.

- 11) K. Okitsu, Y. Hayakawa, T. Yamaguchi, M. Kumagawa, A. Hirata, S. Fujiwara, Y. Okano, N. Imaishi, S. Yoda and T. Oida: *Cryst. Res., Technol.* **31** (1996) 969.
- 12) Y. Hayakawa, K. Balakrishnan, H. Komatsu, N. Murakami, T. Nakamura, T. Koyama, T. Ozawa, Y. Okano, M. Miyazawa, S. Dost, L.H. Dao and M. Kumagawa: *J. Cryst. Growth*, **237-239** (2002) 1831.
- 13) Y. Hayakawa, Y. Okano, A. Hirata, N. Imaishi, Y. Kumagiri, X. Zhong, X. Xie, B. Yuan, F. Wu, H. Liu, T. Yamaguchi and M. Kumagawa: *J. Cryst. Growth*, **213** (2000) 40.
- 14) K. Kinoshita, Y. Arai, Y. Inatomi, T. Tsukada, S. Adachi, H. Mitaya, R. Tanaka, J. Yoshikawa, T. Kaihara, M. Takayanagi and S. Yoda: *J. Cryst. Growth*, **388** (2014) 12.
- 15) K. Kinoshita, Y. Arai, Y. Inatomi, T. Tsukada, S. Adachi, H. Mitaya, R. Tanaka, J. Yoshikawa, T. Kaihara, M. Takayanagi and S. Yoda: *J. Cryst. Growth*, **419** (2015) 47.
- 16) K. Sakata, M. Mukai, M. Arivanandhan, G. Rajesh, T. Ishikawa, Y. Inatomi and Y. Hayakawa: *Trans. JSASS Aerospace Tech.*, **12** (2014)31.
- 17) H. Mirsandi, T. Yamamoto, Y. Takagi, Y. Okano, Y. Inatomi, Y. Hayakawa and S. Dost: *Microgravity Sci. Technol.*, **27** (2015) 313.
- 18) X. Jin, H. Mirsandi, T. Yamamoto, Y. Takagi, Y. Okano, Y. Inatomi, Y. Hayakawa and S. Dost: *JJAP Conf. Proc.*, **4** (2016) 011107.
- 19) Y. Inatomi, K. Sakata, M. Arivanandhan, G. Rajesh, V. Nirmal Kumar, T. Koyama, T. Ozawa, Y. Okano and Y. Hayakawa: *npj Microgravity*, **1** (2015) 15011.
- 20) V. Nirmal Kumar, M. Arivanandhan, G. Rajesh, T. Koyama, Y. Momose, K. Sakata, T. Ozawa, Y. Okano, Y. Inatomi and Y. Hayakawa: *npj Microgravity*, **2** (2016) 16026.
- 21) G.Rajesh, M.Arivanandhan, N.Suzuki, A.Tanaka, H.Morii, T.Aoki, T.Koyama, Y.Momose, T.Ozawa, Y.Inatomi, Y.Takagi, Y.Okano and Y.Hayakawa: *J. Cryst. Growth*, **324** (2011) 157.

"Reprinted from the Publications listed below with permission from npj Microgravity."

1. Y. Inatomi, K. Sakata, M. Arivanandhan, G. Rajesh, V. Nirmal Kumar, T. Koyama, T. Ozawa, Y. Okano and Y. Hayakawa: *npj Microgravity*, **1** (2015) 15011.
2. V. Nirmal Kumar, M. Arivanandhan, G. Rajesh, T. Koyama, Y. Momose, K. Sakata, T. Ozawa, Y. Okano, Y. Inatomi and Y. Hayakawa: *npj Microgravity*, **2** (2016) 16026.